Composite Structures 336 (2024) 118005

Contents lists available at ScienceDirect

Composite Structures

journal homepage: www.elsevier.com/locate/compstruct

Numerical investigation of internal damage in heterogeneous-structured laminates using a 3D multiple physical mechanisms based constitutive model

Shuai Zhu [a], Emmanuel Brousseau [a,*], Yiyu Shao [b,c], Wenfei Peng [b,c]

[a] Cardiff School of Engineering, Cardiff University, Cardiff CF24 3AA, United Kingdom
[b] Faculty of Mechanical Engineering and Mechanics, Ningbo University, 818 Fenghua Road, Ningbo 315211, China
[c] Zhejiang Provincial Key Lab of Part Rolling Technology, Ningbo University, 818 Fenghua Road, Ningbo 315211, China

ARTICLE INFO

Keywords:
Heterogeneous-structured laminates
Interface affected zone
Dislocations
Back stress
Strain hardening

ABSTRACT

Heterogeneous-structured laminates (HSLs), which consist of multiple layers of metallic materials arranged in successive pairs of coarse-grained (CG) and nano-grained (NG) layers, have been recently reported to display excellent balance of strength and ductility. However, it is argued that accompanying state-of-art numerical models developed to simulate the deformation of this specific class of composite materials have limitations for investigating their underlying damage evolution. Addressing this issue is essential to support the rational design, optimisation and application of HSLs, especially when subjected to contact and dynamic processes. For this reason, a novel 3D numerical framework for HSLs is proposed and tested in this research considering published experimental findings and dislocation theories. This framework comprehensively considers the evolution of various types of dislocations and back stress while being coupled with the Johnson Cook damage criterion. The HSL specimens simulated here were made of alternating layers of CG and NG copper separated by interface affected zones. Following initial microhardness and uniaxial tensile simulations on homogenous copper with different grain sizes, simulations of HSLs were conducted to study the effect of different layer thickness and the volume fraction of the NG layer. Overall, a good correlation between numerical and experimental results was achieved. An important and distinguishing characteristic of this research is that the proposed model enables the evolution of internal damage and the synergetic effect between the CG and NG layers to be investigated. Through the evaluation of the damage accumulation factor in the NG layer, the simulations results yielded quantitative information which aligned with the following known experimental observations: 1) the smaller the layer thickness, then the smaller the internal damage and 2) the internal damage increases with the increase in volume content of the NG layer. In addition, for a set simulated strain of 10%, the developed model could be used to show that the damage accumulation factor in the NG layer was 10 times lower than that in its counterpart, i.e., a stand-alone NG layer not sandwiched between two CG layers.

1. Introduction

Heterogeneous-structured laminates (HSLs) are a class of composite materials made of stacks of metallic layers where each layer exhibits a homogenous grain size distribution and where the series of two successive layers consists of a coarse-grained (CG) and of a nano-grained (NG) layer. HSLs have been reported to display excellent material properties and the potential to achieve an advantageous strength-ductility trade-off [1–4]. The interesting property of HSLs originates from the synergy between the successive CG and NG stacked layers as the CG layer exhibits remarkable ductility but low yield strength, while its NG counterpart is associated with reduced ductility but increased yield strength [5]. When under strain, this significant difference in the mechanical response between layers leads to the formation of interface affected zones (IAZs). More specifically, an IAZ, which is located near the interface in a CG layer, exhibits a large number of dislocations and resulting back stress. The size of an IAZ is typically on the order of 5 μm to 6 μm [1], or the size of a coarse grain [6], and is believed to play a crucial role in the strengthening of such laminate materials. It was also reported that the tensile yield strength of HSLs increases significantly

* Corresponding author.
E-mail address: BrousseauE@cardiff.ac.uk (E. Brousseau).

https://doi.org/10.1016/j.compstruct.2024.118005
Received 29 October 2023; Received in revised form 23 January 2024; Accepted 29 February 2024
Available online 9 March 2024

with decreasing layer thickness [1]. However, its uniform elongation was found to be non-monotonic and changes as a function of layer thickness [1,3,7,8]. This means that there is an optimum value for the layer thickness of HSLs and more systematic studies are required to identify such ideal design configuration depending on the specific material, or combination of materials, considered in such composite laminates.

A number of experimental efforts have been reported in the literature to study the structural properties of HSLs [4,5]. Such investigations include that of Ma and co-workers who fabricated HSLs using high-pressure torsion, rolling and annealing [7]. These authors found that different volume content of the NG layers and the resulting IAZs were crucial in determining the tensile deformation behaviour of HSLs. In addition, Huang et al. further investigated the deformation mechanism of HSLs using an in-situ micro tensile set-up combined with digital image correlation [1]. These authors found that the thickness of the layers should be about twice that of the IAZs to achieve optimal design in terms of strength-ductility trade-off. When studying the strengthening behaviour and attempting the quantitative prediction of the laminate properties, the rule of mixture (ROM) has generally been adopted by the research community [7,9–11]. However, it should be noted that only the parameters CG and NG volume contents are considered when implementing the ROM method and the actual layer thickness is not taken into account. As a result, for a given ratio of volume content, the outcome of the ROM method is constant regardless of the change in layer thickness. This is a limitation of the ROM approach because, as reported in the experimental data from Huang and co-workers [1], the tensile strength of HSLs depends on the layer thickness for a given volume content. In addition, the ROM method is only applicable when the layer thickness is relatively large and the volume content of the IAZs is negligible [7]. Besides, a larger hardening than that predicted by the ROM method was observed by Ma et al. [7]. Thus, it is argued that there is still a need for further research to develop our understanding and modelling of the underlying strengthening mechanisms and the evolution of internal damage in HSLs such that the optimum design of these types of composite structures can be achieved.

In addition to uniaxial tensile experiments mentioned above, nano/micro indentation is also an important material characterisation method where only a small-scale sample is needed rather than a large-scale specimen [12,13]. Nano/micro indentation testing can thus be an appropriate alternative to large scale experiments especially when these can be difficult and complex to conduct or when material cost is an issue [14,15]. Characterizing the hardness of HSLs is important as it is also a key material parameter[5]. However, only a few experimental reports have focussed on this material property for HSLs and none from a numerical modelling viewpoint. Huang et al. investigated the nano-indentation hardness of a copper-based HSL using a Berkovich indenter [1], while Ma et al. [3,7] and Wang et al. [16] used a Vickers indenter to study the nanoindentation hardness of copper/bronze HSLs. Overall, these experiments revealed that the microstructure and composition difference across the interface between layers can result in a significant variation in hardness.

Numerical modelling is a flexible and efficient tool, which could be used effectively to predict the hardness and other mechanical properties of various HSL compositions during the design stage of these laminate structures. Crystal Plasticity Finite Element Method (CPFEM), in which the real topology of grains can be accounted for, is potentially of interest in this context as the method could enable the consideration and modelling of multiple grains within HSLs [17]. However, the actual size of such a multiple-layered structure is typically in the order of several or tens of millimetres at least. This means that a CPFEM model of HSLs can be composed of hundreds and even thousands of grains, making this method computationally prohibitive. While two-dimensional (2D) CPFEM with an homogenization scheme has been used to alleviate this issue [18], most of the current CPFEM-based numerical attempts to model HSLs mainly focus on the geometric topological relationship of grains and their interactions and do not provide sufficient insight into fundamental deformation mechanisms, such as dislocation activities and back stress. The Molecular Dynamics (MD) method can also be adopted to investigate the mechanical response of gradient structures as reported by Fang and co-workers [19]. More specifically, these authors employed a 2D model to address constraints of computational efficiency and mismatch on the spatiotemporal level since the consideration of only tens of grains would otherwise be achievable in a typical 3D MD model. Despite the efforts presented by these authors, the classical MD method remains not well suited for the quantitative investigation of dislocation activities and back stress observed during experiments. Yuan and Du developed an analytical model for heterogeneous laminates and revealed their hardening mechanism [20]. Another analytical model for gradient-nanostructured 304 stainless steels was proposed by Zhu and co-workers by taking into account the depth-dependent grain size and nano scale structure [68]. The predictions obtained by these authors agreed well with experimental results in terms of yield stress, ductility and strain hardening rate. In spite of this, analytical methods have typical limitations for investigating the spatial distribution of field variables and are restricted to the modelling of relatively simple deformation scenarios. Some researchers, such as Wu et al. [21], employed the traditional finite element method (FEM) to investigate stress, strain and strain gradient distributions across the thickness direction of gradient steel. The constitutive models used by these authors for the CG and gradient layers were obtained by fitting uniaxial tensile stress–strain data on individual layers. Although the extra strengthening of the composite laminates was modelled when considering the stack of these layers, the exact underlying deformation mechanisms at play were not fully elucidated. Li and co-workers developed a dislocation density-based theoretical model and investigated the mechanical behaviour of gradient structures [22]. Experiments and FEM modelling were further employed by Li et al. to study the strength-ductility synergy of gradient structures [23]. Although multiple mechanisms, including geometrically necessary dislocation (GNDs) and back stress, were considered by these authors, the FEM model developed was limited to conducting 2D analyses. Zhao et al. presented a constitutive FEM model considering the deformation heterogeneities and multiple related mechanisms, such as dislocations and back stress strengthening [6]. The effect of grain size, layer thickness and the NG layer volume content were thoroughly investigated and compared with experimental data. However, the failure criteria and the study of the microhardness were not included in this work. Besides, the numerical framework adopted by these authors would not be well suited if one was to follow it for simulating dynamic processes. Thus, the development of a multiple physical mechanisms based constitutive model coupled with damage criterion is essential for investigating the fundamental principles governing the deformation behaviour of HSLs and especially when subjected to dynamic processes.

Quantitatively, experimental reports also indicate that the uniform deformation of a NG layer in the laminates is at least ten times higher than that of its a stand-alone counterpart [7,24]. Based on this, in the classical ROM approach, or with the modified ROM method proposed in Zhao et al. [6], the engineering stress of the NG layer in the laminates is assumed to be constant after necking. Although a reasonable correlation between experimental and predicted results was observed when adopting this assumption in the case of HSLs displaying a relatively large layer thickness, the prediction accuracy of this approach reduces as the layer thickness decreases. While it can indeed be said that the NG layer in the laminate is much stronger than when it is considered standalone, it is questionable to assume that its engineering stress remains constant after necking when developing a numerical model of HSLs. For this reason, not only it is important to take into account of multiple physical mechanisms when developing a constitutive model of HSLs, it is also essential to include a failure criterion when developing an integrated FEM model of HSLs. The Johnson Cook (JC) failure criterion [25], which was initially proposed for macroscopic metal failure, has proven to be

robust and efficient for simulating metal deformation processes on the microscale [26–29]. This is due to its comprehensive inclusion of the effect of strain, strain rate and temperature. Thus, given the limitations of the current numerical methods reported above for modelling HSLs, it is proposed that the JC failure criterion is also considered when numerically simulating the indentation and uniaxial tensile responses of HSL materials.

In summary, despite recent experimental and numerical progress, the deformation mechanism of HSLs, and the corresponding evolution of dislocations and back stress, remains unclear. Besides, to realize the numerical simulation of HSLs when subjected to dynamic deformation processes, a framework coupled with damage criterion is needed. This is because the quantitative characterisation of internal damage when simulating such structures remains a gap in the current state of the art. It is also argued that the further understanding of strengthening and damage mechanisms of HSLs should lead to the enhanced tailoring and design of these materials such that their promising strength-ductility synergy can be taken full advantage of. An efficient and robust physical mechanisms-based 3D numerical method coupled with a failure criterion remains to be developed to address this gap. This is particularly important considering the large design space that is typical of HSLs, i.e., material employed, layer thickness and the respective grain size of the CG and NG layers. For this reason, this work aims to develop such a constitutive model to quantitatively investigate the sources of hardening and the internal damage evolution of HSLs and to predict the response of such laminate materials under a range of deformation scenarios, including in tension and during nanoindentation.

The remainder of this paper is organised as follows: the constitutive model for the NG and CG layers as well as the IAZ, the JC failure criterion and the numerical implementation process are introduced in section 2. In section 3, indentation and tensile simulations on homogenous grained copper are carried out first to validate the correctness and robustness of the developed numerical framework. Then, the effect of the layer thickness and the NG volume content on the mechanical response of HSLs are investigated. Calculations that rely on the ROM method and the model prediction method proposed by Zhao and co-workers [6] are also conducted and compared against those published in the literature to further validate the accuracy of the numerical work reported here. Finally, in the last part of section 3, the distinguishing characteristic of this research, i.e., the developed integrated FEM model, which combines the multiple physical mechanisms based constitutive model coupled with the JC damage criterion, is implemented to study the synergistic effect and mutual constraints of the NG and CG layers in the laminates as well as the damage evolution during the deformation process. Conclusions and issues needing further investigation are then presented in section 4.

2. Numerical framework and FEM model

2.1. Multiple mechanisms based constitutive model

Considering the significant dislocation activity experimentally observed in the deformation process of laminates and the relative ease of numerically implementing the conventional mechanism-based strain gradient (CMSG) theory, the deformation response and strengthening mechanism of HSLs were investigated based on the CMSG [30] and dislocation pile-up [31] theories in this research. The flow stress is related not only to the statistically stored dislocations (SSDs) but also to the GNDs from the sample level, the grain level and the back stress. This direct introduction of dislocations into the constitutive model does not require the need to consider higher order stresses and boundary conditions [32–34] and thus, can be implemented within the VUHARD/VUSDFLD subroutines, which are mathematically easier than the UEL/VUEL and VUMAT/UMAT subroutines [35,36]. A multiscale schematic of the developed model is shown in Fig. 1 and the associated constitutive equations are presented in the following sub-sections.

2.1.1. Constitutive model for homogenous layers

The Taylor hardening law [37] was adopted in the presented work to relate the flow stress with the dislocation density. The dislocation density can be further decomposed into the SSD density, ρ_{SSDs}, and the GND density, ρ_{GNDs}. The flow stress σ_{f} is defined as [6]:

$$\sigma_{\mathrm{f}} = \sigma_0 + M\alpha Gb\sqrt{\rho_{\mathrm{SSDs}} + \rho_{\mathrm{GNDs}}} + \sigma^b \tag{1}$$

where σ_0 is the lattice friction stress, M is the Taylor factor, α is a material constant, G is the shear modulus, b is the magnitude of the Burgers vector and σ^b is the back stress. Considering the significant amount of back stress observed experimentally and following the work of [6,31,38], the back stress σ^b is defined as:

$$\sigma^b = \frac{MGb}{\pi(1-\upsilon)d}N \tag{2}$$

where d is the grain size, υ is the Poisson's ratio, N is the dislocation number within a pile-up. The rate of change of N is defined following the work of [39].

$$\dot{N} = N_\Delta\left(\frac{2}{3}\dot{\epsilon}^p - \frac{N}{N^*}\dot{p}\right) \tag{3}$$

Considering the negligible effect of the plastic strain components $\dot{\epsilon}^p$

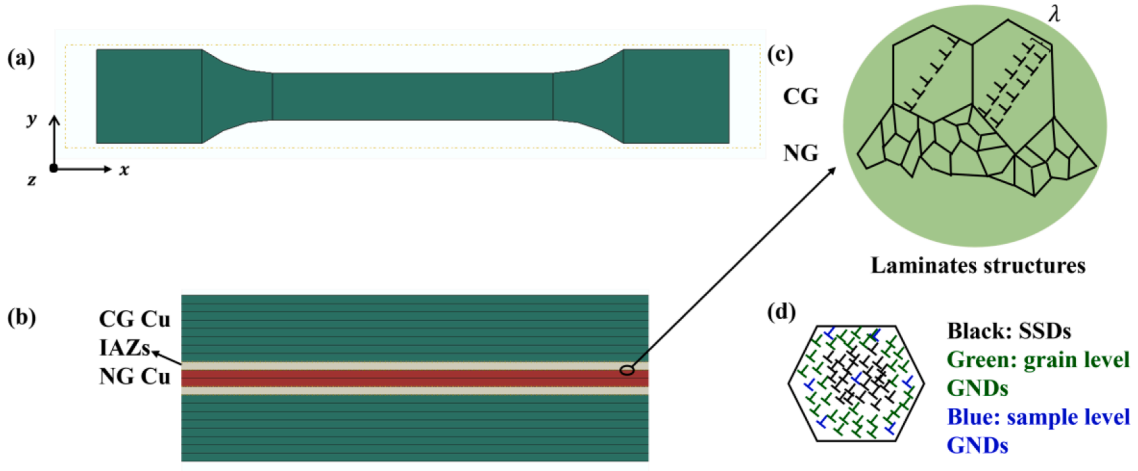

Fig. 1. (a) Schematic diagram of the modelled tensile dog-bone specimen; (b) layers of the integrated FEM model with a NG volume content of 10 %; (c) schematic of piled-up GNDs near the boundaries of NG and CG layer; (d) schematic of the various dislocations considered in the presented work.

and to ease the implementation process, equation (3) is simplified as:

$$\dot{N} = N_{\Delta}\dot{p}\left(\frac{2}{3} - \frac{N}{N^{*}}\right) \tag{4}$$

where N_{Δ} is the initial evolution rate of N, N^{*} is the saturated pile-up dislocation number and $\dot{p}$ is the equivalent plastic strain rate. N^{*} and N_{Δ} are defined with equation (5) and (6) respectively [6]:

$$N^{*} = \frac{\pi(1-\nu)k_{\mathrm{HP}}}{MGb}d^{\frac{1}{2}} \tag{5}$$

$$N_{\Delta} = \frac{4M\lambda}{3b} \tag{6}$$

where k_{HP} is the Hall-Petch constant and λ is the distance between slip lines as shown in Fig. 1(c).

During the deformation process, apart from the back stress, the dislocation hardening is also caused by the interactions between dislocations as shown in Fig. 1(d). This dislocation hardening behaviour is included in the presented work as stated in equation (1). The density of piled-up GNDs is defined on both the sample level and the grain level as:

$$\rho_{\mathrm{GNDs}} = \rho^{\mathrm{sam}}_{\mathrm{GNDs}} + \rho^{\mathrm{gra}}_{\mathrm{GNDs}} \tag{7}$$

where $\rho^{\mathrm{sam}}_{\mathrm{GNDs}}, \rho^{\mathrm{gra}}_{\mathrm{GNDs}}$ are the sample level and the grain level GNDs density, respectively. The grain level GNDs density is defined as [6]:

$$\rho^{\mathrm{gra}}_{\mathrm{GNDs}} = \frac{d}{\lambda}\frac{N}{d^{2}} \tag{8}$$

where $\frac{d}{\lambda}$ is the number of pile-ups in a grain.

Apart from the GNDs for the grain level, the non-uniform strain gradient is also generated via dislocation pile-up [3] which would lead to the size effect. The layer thickness studied in the experiments can be as thin as 3.7 μm [1] and the smallest nanoscale grain size is 100 nm. Therefore, the effect of GNDs on the sample level, although expected to be not that significant in tensile loading scenarios, is also included in this work and defined following the work in [40,41].

$$\rho^{sam}_{GNDs} = \frac{\bar{r}\eta^{p}}{b} \tag{9}$$

where $\bar{r}$ is Nye's factor [40] and η^{p} is the strain gradient, which can be calculated using $\Delta\eta^{p} = \sqrt{\frac{1}{4}\Delta\eta^{p}_{ijk}\Delta\eta^{p}_{ijk}}$ [42] and $\Delta\eta^{p}_{ijk}$ are strain gradient components.

A modified Kocks-Mecking-Estrin (KME) model [43–45], proposed by Li et al. [22], is adopted in this work to describe the evolution of SSDs for both the CG and NG phases.

$$\frac{\partial\rho_{\mathrm{SSDs}}}{\partial\varepsilon^{p}} = M\left[\frac{k^{g}_{\mathrm{mfp}}}{bd} + \frac{k^{\mathrm{dis}}_{\mathrm{mfp}}}{b}\sqrt{\rho_{\mathrm{SSDs}} + \rho_{\mathrm{GNDs}}} - k_{\mathrm{ann}}\left(\frac{\dot{\varepsilon}^{\mathrm{p}}}{\dot{\varepsilon}_{\mathrm{ref}}}\right)^{-\frac{1}{n_0}}\rho_{\mathrm{SSDs}} - \left(\frac{d_{\mathrm{ref}}}{d}\right)^{2}\rho_{\mathrm{SSDs}}\right] \tag{10}$$

where k^{g}_{mfp} and $k^{\mathrm{dis}}_{\mathrm{mfp}}$ are geometric factor and proportional factor that control the dislocation activities at the grain boundaries and the dislocation reactions on the dislocation mean free path (MFP), $\dot{\varepsilon}_{\mathrm{ref}}$ is the reference strain rate and d_{ref} is the reference grain size, k_{ann} is the dislocation annihilation factor, $k_{\mathrm{ann}}\left(\frac{\dot{\varepsilon}^{\mathrm{p}}}{\dot{\varepsilon}_{\mathrm{ref}}}\right)^{-\frac{1}{n_0}}\rho_{\mathrm{SSDs}}$ is the annihilation rate, $\dot{\varepsilon}^{\mathrm{p}}$ is plastic strain rate and n_0 is dynamic recovery exponent.

2.1.2. Constitutive model for interface affected zones (IAZs)

In this work, the thickness values considered for the CG layer were 4.8 μm and 4 μm, while it was 100 nm for the NG layers to ensure that the simulations aligned with the experiments reported in [1,7] for comparison purpose. This significant difference in grain size leads to a mechanical incompatibility between interfaces during plastic deformation and further results in high GND density, strain gradient [5] and back stress [46]. The dislocation ledge source theory [47] states that NG-CG interfaces could act as sources of dislocations. Experiments show that there exists a 'one grain width zone' (about 5 μm to 6 μm) in the CG layer near the NG-CG interface where the GND density is higher than in other parts of that layer [2–4]. This zone is called the IAZ. The dislocation pile-up behaviour in the IAZs is different from that in the homogenous layers due to the significant difference in layer properties as reported above. Following the work of Zhao et al. [6], the dislocation number within a pile-up for an IAZ is defined as:

$$N^{*}_{\mathrm{IAZ}} = \frac{\pi(1-\nu)\left(k_{\mathrm{HP}}d^{-\frac{1}{2}}_{\mathrm{NG}} + \Delta\sigma_{0}\right)}{MGb}d_{\mathrm{CG}} \tag{11}$$

where d_{NG} is the size of a nano grain and d_{CG} is the size of a coarse grain, $\Delta\sigma_{0}$ is the difference of lattice friction stress between the NG and the CG layers. Comparing equation (11) with equation (5), a larger dislocation pile-up is produced in the IAZ region, which would further lead to a larger back stress.

2.2. Johnson Cook failure criterion

As stated by Zhao et al. [6], a reasonable damage and failure model should be developed to investigate the synergistic behaviour of the NG and CG layers in HSLs. Herein, the JC dynamic failure model, which is proved to be robust in microscale processes affected by large deformations [26,27], was adopted as the failure criterion. The JC failure model comprehensively includes the effect of strain hardening, strain rate and temperature. More specifically, the JC failure model is based on the calculation of the equivalent plastic strain, which is expressed as follows:

$$\bar{\varepsilon}^{pl}_{f} = (d_1 + d_2 e^{d_3\gamma})(1 + d_4\ln(\frac{\dot{\bar{\varepsilon}}^{pl}}{\dot{\varepsilon}_0}))(1 + d_5\frac{T - T_r}{T_m - T_r}) \tag{12}$$

where d_1 to d_5 are material damage parameters, γ is the stress triaxiality ratio, $\dot{\bar{\varepsilon}}^{pl}$ is the equivalent plastic strain rate, $\dot{\varepsilon}_0$ is the equivalent reference strain rate, T is the current temperature, T_r is the reference temperature and T_m is the material melting temperature. A summation of incremental failure strain $\Delta\bar{\varepsilon}^{pl}_{f}$ is performed over all increments to calculate the failure criterion, ω, as follows [25]:

$$\omega = \Sigma\left(\frac{\Delta\bar{\varepsilon}^{pl}_{f}}{\bar{\varepsilon}^{pl}_{f}}\right) \tag{13}$$

where $\bar{\varepsilon}^{pl}_{f}$ is equivalent plastic strain. Failure is considered to be reached when the JC failure criterion, ω, increases to a value equal to "1". The damage parameters used in this work were those defined for copper [25].

2.3. Implementation and finite element modelling

The constitutive model and JC failure criterion introduced in the previous section were implemented via user-defined subroutine VUHARD/VUSDFLD and thus, can be used with ABAQUS/EXPLICIT. The implementation flow chart is displayed as shown in Fig. 2. The microhardness of homogenous grained layers, i.e., the NG and CG layers were also investigated numerically using a Berkovich pyramid indenter following the work reported in [1]. The imperfection of the tip, i.e., the tip bluntness as well as the friction between the indenter and the specimen, were also taken into account based on the work of [48–50]. The indentation speed was set to 10 μm /s and the indentation depth was 10 μm. The schematic diagram of the FEM model for indentation is shown

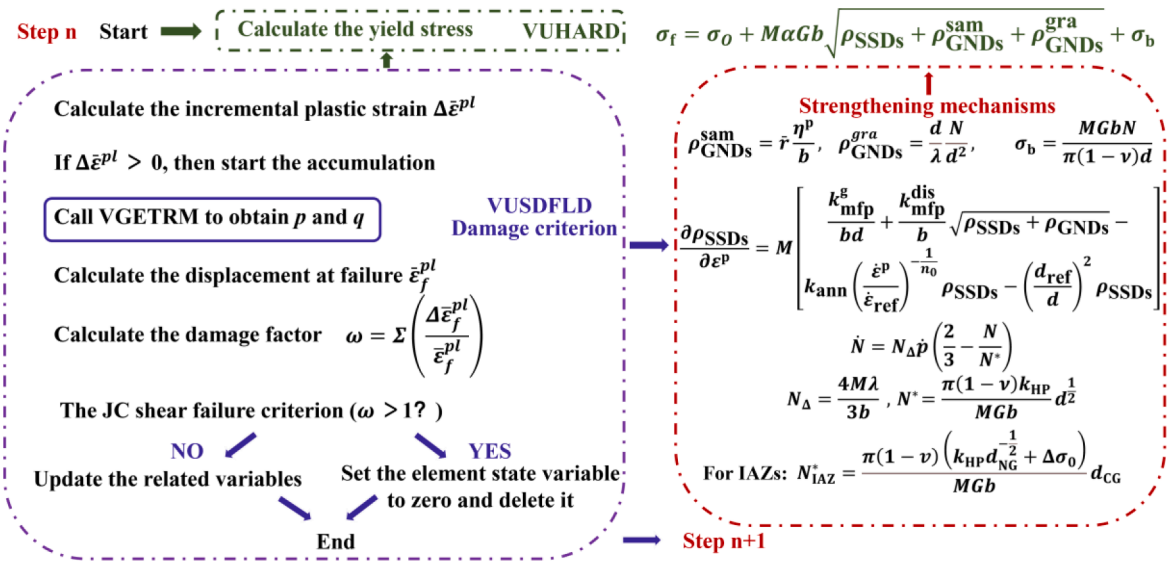

Fig. 2. Flow chart of the developed 3D multiple physical mechanisms algorithm.

in Fig. 3. The dimension of the dog-bone shaped specimen for the uniaxial tensile simulations on homogenous copper (section 3.2) and for the subsequent integrated FEM modelling (section 3.3.3) was set following the reports in [1] and [7], respectively. The gauge section consisted of three zones, i.e., the NG layer, the CG layer and the IAZ zone as shown in Fig. 1(a) and 1(b). The specimen was discretised using C3D8 elements, and the gauge section was refined to ensure mesh independence on the simulated results. The strain rate was set to 5×10^{-4} [1] and the material properties in the constitutive model parameters were sourced from published data as listed in Table 1. The stress (in the S11 and S22 directions), strain and all the state variables discussed in this work were calculated using the average value of the gauge section. A Python script was compiled to extract the variables and plot the results for comparison with experimental data.

3. Results and discussion

3.1. Microhardness simulation on standalone homogeneous grained layers

Microhardness simulations of homogenous grained layer with grain size of 4.8 μm and 100 nm were conducted using the developed framework. The simulated load–displacement curves are shown in Fig. 4 (a). From the respective curves, it is obvious that the reaction force of the NG copper is significantly higher than that of the CG layer, as expected. The numerical micro indentation hardness H_i was calculated as $H_i = \frac{F_N}{A_p}$, where F_N is the normal reaction force and A_p is the projected area. The calculated results are shown in Fig. 4(b) together with the

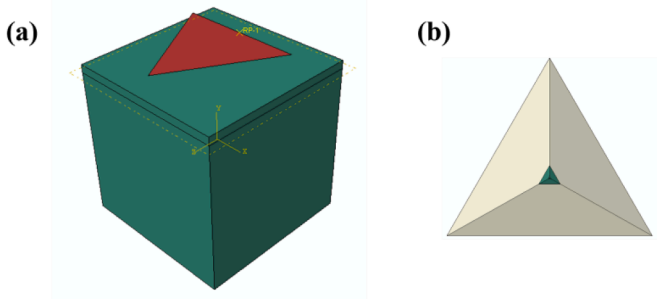

Fig. 3. (a) FEM model of indentation; (b) detailed Berkovich indenter with consideration of tip bluntness.

Table 1
Material properties:

Parameter	Symbol	Value
Young's modulus (GPa)	E	200
Shear modulus (GPa) [22]	G	42.1
Poisson's ratio [22]	υ	0.36
Magnitude of the burgers vector (nm)	b	0.256
Lattice friction stress (MPa) [51]	σ_0	0 (CG copper) 31.8 (NG copper)
Hall-Petch constant (MPa·$\mu m^{1/2}$) [22]	k_{HP}	110
Geometric factor [6]	k_{mfp}^g	0.2
Proportionality factor [6]	k_{mfp}^{dis}	0.02
Dynamic recovery constant [6]	k_{ann}^0	2.1
Dynamic recovery exponent [22]	n_0	21.25
References strain rate (s^{-1}) [22]	$\dot{\varepsilon}_{ref}$	1
Reference grain size (μm) [6]	d_{ref}	1.5
Distance between slip lines (nm) [6]	λ	260
Initial dislocation density (m^{-2}) [6]	ρ_0	10^{13}
Johnson Cook damage parameters [25]	d_1	0.54
	d_2	4.89
	d_3	−3.03
	d_4	0.014
	d_5	1.12

experimentally obtained hardness values from [1]. The numerical results correlate well with the experimental data as the simulated micro indentation hardness for the CG and the NG layer were 0.79 GPa and 2.43 GPa, respectively. The observation of the experimental data in this figure highlights the abrupt change in hardness between the different layers showing a prominent difference in material properties. The good correlation between the numerical and experimental results shows that the developed framework may not only be used in tensile simulations, but also in dynamic indentation process where relatively large compression and damage of material are involved.

3.2. Uniaxial tensile responses of standalone homogenous NG and CG copper layers

To further test the suitability of the developed numerical framework, uniaxial tensile simulations on homogenous grained copper were also carried out. The simulated stress–strain curves for copper with grain sizes of 4.8 μm, 4 μm and 100 nm are displayed in Fig. 5(a). The experimental results reported in [1] and [7] are also plotted for comparison. It is observed from this figure that the simulated results agree

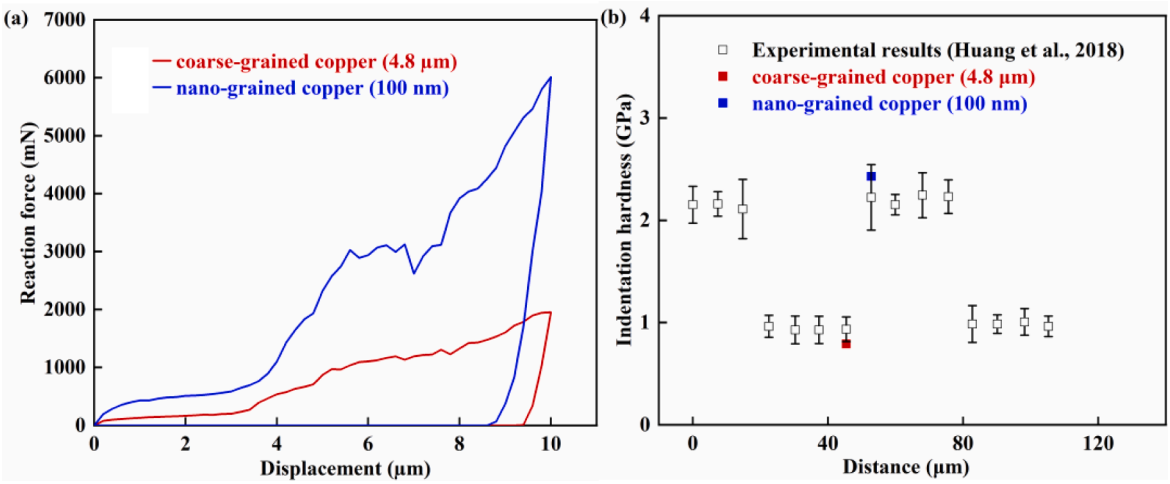

Fig. 4. (a) Simulated reaction force–displacement curves during indentation and (b) comparison between numerical and experimental microhardness values for homogenous-grained CG and NG copper.

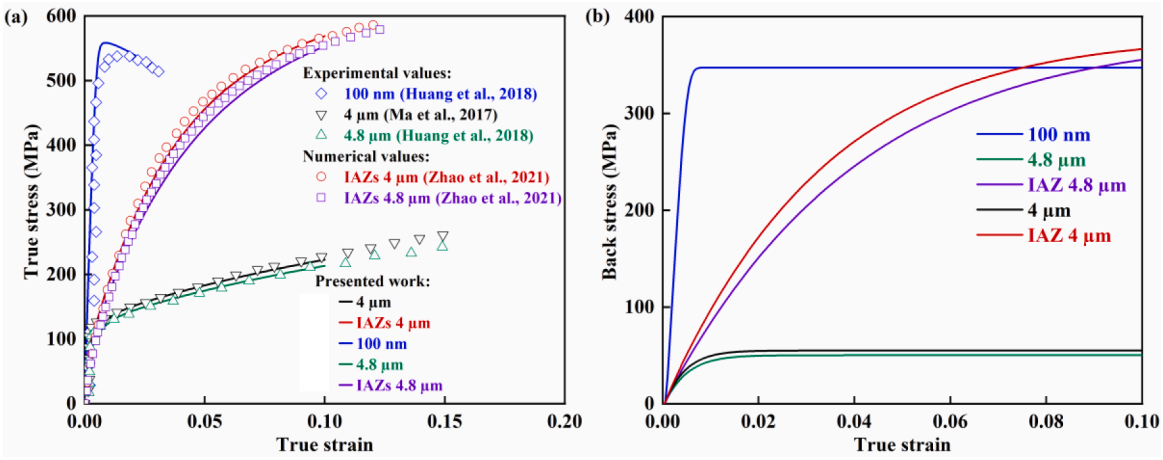

Fig. 5. Simulated and experimental (a) true stress-true strain curves (b) back stress-true strain for homogenous-grained copper with grain sizes of 100 nm, 4 μm and 4.8 μm and for the IAZ.

well with the experimental data. One should notice that the IAZ data provided in this figure are merely for demonstration purpose as such a zone can only exist due to the interaction between the NG and CG layers. However, the IAZ results obtained in this simulation can still be compared against those reported in the simulation from [6] and thus, they are also included in the plot of Fig. 5(a). It can be seen that the displayed stress–strain curves exhibit a strong grain size dependent behaviour. The NG copper shows no strain hardening and fails immediately after yield, i.e., around 530 MPa. This simulated behaviour agrees well with the experimental findings of [52–55] for nanograined copper and also with those of [56] who investigated nanograined Ni. In contrast, and as expected, the stress in the CG layer keeps increasing with the applied strain post yield and although the value of stress is significantly lower than that in NG layer, a better ductility is observed.

The back stress was also output as a state variable and compared with the experimental values measured with the unloading–reloading experiments of [1]. In particular, the evolution of back stress of homogenous copper layers with different grain size is displayed in Fig. 5(b) to quantitively explain the significant contribution of back stress to the mechanical response. The back stress strengthening, or in other words the contribution of the back stress, is significantly higher than that of the effective stress caused by pure dislocation density strengthening (see equation 1). The back stress is mainly caused by the GNDs generated within each layer and piled-up near the interfaces, i.e., IAZs. From Fig. 5 (b), it is observed that the back stress in the NG and CG layers saturates rapidly after initial yielding. In contrast, the back stress value of the IAZ keeps on increasing due to the continuous increase in piled-up dislocations. The simulated data suggest that the stress and back stress level of the IAZs can be as high as that in the NG layer when the strain is around 8 %. This indicates that the IAZs are crucial in the hardening behaviour of HSLs. It can also been seen from this figure that the back stress in the NG layer saturates around 347 MPa, which is in close alignment with the experimental results presented in [16] and with the numerical results found in [6].

The deformation at 10 % tensile strain for these three homogeneous standalone specimens taking into account of the JC damage factor are displayed in Fig. 6. The necking is only observed in the NG layer, which indicates an early failure as was highlighted above with the data plotted in Fig. 5(a). The corresponding JC damage accumulation factor at 10 % tensile strain in the NG layer, in the 4 μm CG layer and the 4.8 μm CG layer was found to be 0.06, 0.0064 and 0.0063, respectively. This shows quantitatively that the damage factor in the NG layer is one order of magnitude larger than that in the CG layers for this given percentage of tensile strain. These different damage conditions are the result of the smaller grain size in the NG layer, which leads to this layer not being able to sustain dislocation accumulation. However, when such a layer is not standalone, i.e., when it is within a laminate structure, experimental results reported in the literature suggests that such stress concentration

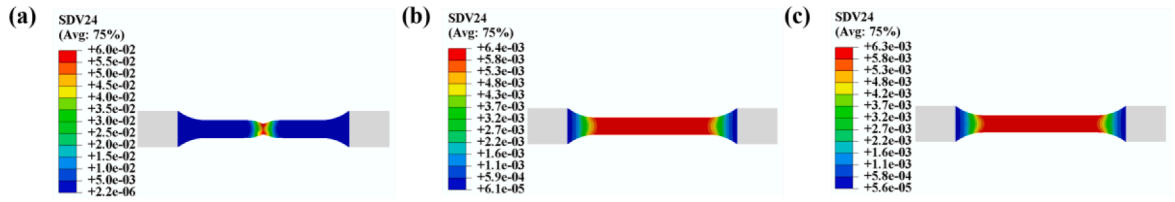

Fig. 6. Specimen deformation and corresponding JC damage accumulation factor, Solution-Dependent State Variables (SDV) 24 at 10 % tensile strain for homogenous copper layers with grain size of (a) 100 nm (b) 4 μm and (c) 4.8 μm.

is reduced through the motion of dislocations in the CG layer near the interface i.e., the IAZ. Such dislocation-induced back stress and dislocation hardening explains why the stress in the IAZ keeps increasing with the strain as shown in Fig. 5(b).

3.3. Uniaxial tensile response of HSLs

The closeness of results between the experimental and numerical data obtained with the developed framework for standalone layers as reported in sections 3.1 and 3.2 provides some confidence that the numerical framework could be subsequently applied to further investigate the uniaxial tensile properties of HSLs with different layer thicknesses and NG layer volume content.

As mentioned in section 1, the ROM method has been widely employed to calculate the mechanical response of laminate structures made of different volume contents. When implementing the ROM method [5] for laminated composites, the yield stress, strain hardening, and uniform elongation are calculated as follows:

$$\sigma_{ys} = \sum V_i \sigma'_{i,ys} \tag{14}$$

$$\frac{d\sigma}{d\varepsilon} = \sum V_i \frac{d\sigma_i}{d\varepsilon} \tag{15}$$

$$\varepsilon_{UE} = \frac{\sum V_i \sigma_{i,UE} \varepsilon_{i,UE}}{\sum V_i \sigma_{i,UE}} \tag{16}$$

where V_i is the volume fraction of component i, $\sigma'_{i,ys}$ is the flow stress of component i alone at 0.2 % plastic strain of the composite sample, σ_i is the true stress of component i, σ and ε are the stress and strain of the composite sample and $\sigma_{i,UE}, \varepsilon_{i,UE}$ are true stress and true strain of the sample at necking. As acknowledged earlier from published literature, the yield stress of HSLs using the ROM method correlates well with experimental values when the volume content of the IAZs is relatively low, although the predicted strain hardening rate and uniform elongation are still smaller than the experimentally observed values [5,7].

Because IAZs are not taken into account with the ROM method, Zhao et al. [6] proposed a modified ROM approach as shown in equation (17) for calculating material properties of HSLs samples by volume average over the three regions, i.e. the NG layer, CG layer and the IAZs.

$$\sigma_{\text{laminate}} = \frac{\sigma_{\text{CG}} V_{\text{CG}} + \sigma_{\text{IAZ}} V_{\text{IAZ}} + \sigma_{\text{NG}} V_{\text{NG}}}{V_{\text{total}}} \tag{15}$$

where σ_{laminate} is the stress of the laminate and V_{total} is the total volume of the integrated sample, σ_{CG}, σ_{IAZ} and σ_{NS} are stresses for the three regions and V_{CG}, V_{IAZ} and V_{NG} are the volumes for these respective regions. Good correlation between theoretical modelling and experimental results were obtained by these authors. Therefore, in the following sub-section, the ROM approach and the modified ROM method from Zhao and co-workers [6] are implemented and analysed further.

3.3.1. Effect of layer thickness

It has been widely verified experimentally that the strength-ductility balance of HSLs outperforms their homogeneous grained counterparts and that the layer thickness can be optimised to achieve superior properties [1,57]. Herein, the effect of layer thickness on the tensile response of HSLs composed of copper layers with different thicknesses is investigated. The experimental data reported in [1] and the stress–strain curves simulated with the developed framework for copper-based HSLs with thickness values of 3.7 μm, 7.5 μm, 15 μm, 30 μm, 62 μm and 125 μm are displayed in Fig. 7(a).

From this figure, an obvious layer thickness dependent behaviour is observed. More specifically, a smaller layer thickness leads to a higher stress. This outcome is expected as a smaller layer thickness leads to a higher IAZs density. In the case of the 3.7 μm layer thickness, the IAZs may also overlap. However, this high stress comes at the expense of a reduction in ductility since the effectiveness of back stress hardening is limited. Experiments reported in the literature also show that, during plastic deformation, emitted dislocations at the IAZs span on the order of several micrometres, which is consistent with the fact that the width of an IAZ is also the characteristic length in the strain gradient plasticity theory. Smaller interface spacing means a higher IAZs density which further leads to a higher density of GNDs. The stress concentration is further transmitted from the IAZs to inner parts of CG layer by dislocation activities. When the layer thickness is relatively small, i.e., 3.7 μm, this transmission is hindered by overlapping IAZs. Consecutively, the smaller the layer thickness, the more limited the ductility. The content of IAZs increase from 3.3 % to 100 % when the layer thickness decreases from 125 μm to 3.7 μm. X-ray tomography and digital image correlation data obtained in [58] reveal that the interface between layers in the laminate can act as local stress/strain transformer and delay crack initiation and propagation. It can be seen from Fig. 7(a) that a lower IAZs content, namely when the layer thickness is larger than 15 μm, is associated with a better alignment of experimental and numerical results. On the other hand, when the IAZs content is relatively high, i.e., for layer thicknesses of 3.7 μm and 7.5 μm, obvious deviations can be observed which indicates that appropriate modelling of the IAZs and the interfaces are crucial in the tensile response of laminates.

The simulated results are also plotted and compared with results obtained using the ROM method as shown in Fig. 7(b). As stated earlier, the IAZs are not considered in the ROM method and the volume content the NG and CG layers remain constant, i.e., 50 % for each layer regardless of the changing thickness. This inevitably leads to overlapping predictions using this method as seen in this figure. Besides, this figure illustrates that the ROM-based predictions are smaller than the experimental data. Again, this indicates the crucial role of IAZs in strengthening the laminates.

Considering the significant role that back stress plays in hardening gradient and laminate structures [46,59], the back stress for laminates fabricated with different layer thickness is also analysed in the presented work. In Fig. 8(a), the simulated back stress is plotted and compared with experimental data from [1]. It can be seen that the evolution of the back stress for laminates with the considered layer thicknesses of 7.5 μm and 31 μm agree well with the experiments and that a smaller layer thickness leads to a higher back stress. This is due to the fact that the back stress is mainly caused by GNDs generation and pile-ups near the interfaces. A larger amount of GNDs is expected with larger interface densities i.e., with smaller layer thickness. It can also be observed from Fig. 8(a) that the back stress increases drastically until 1 % true strain

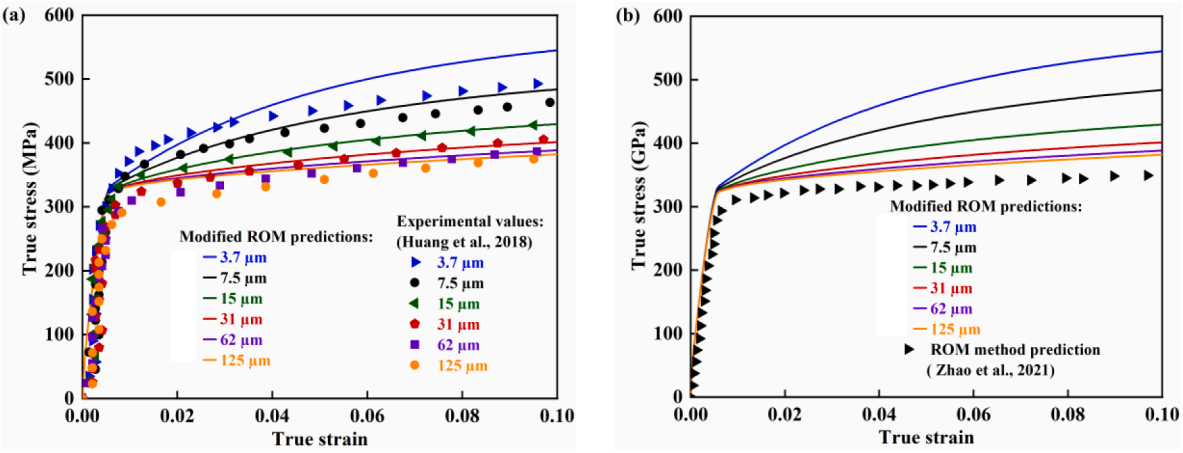

Fig. 7. Plots of simulated stress–strain curves using modified ROM method for copper-based HSL composites with different layer thicknesses against (a) experimental results from [1] and (b) ROM predictions from [6].

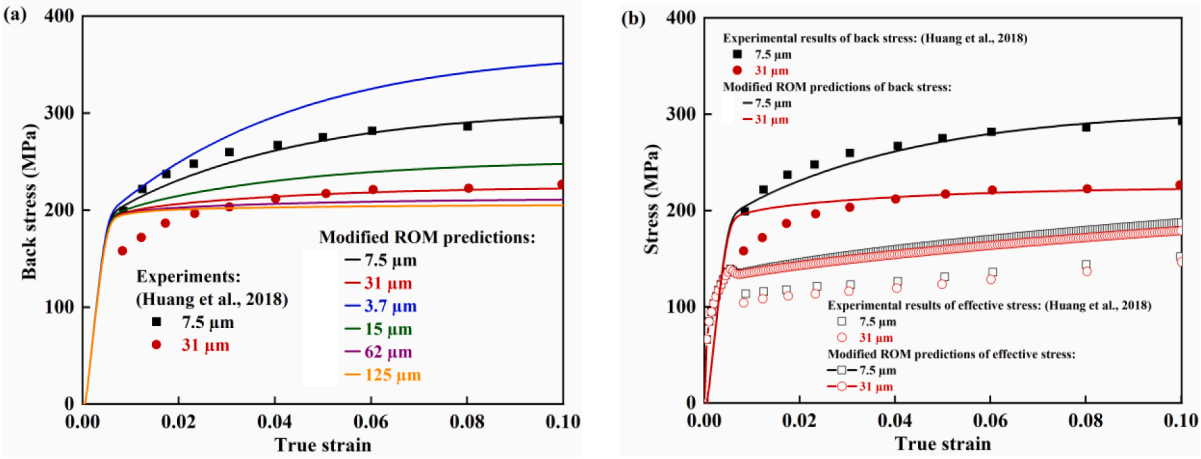

Fig. 8. Evolution of (a) back stress and (b) effective stress for the simulated copper-based HSLs with different layer thickness and comparison with experimental findings from [1].

and tends to saturate afterwards. This indicates that the back stress hardening is most effective in the early stage of deformation, which also correlates well with experimental findings [1]. The calculated effective stress $\alpha Gb\sqrt{\rho}$ [60] is also plotted and compared with experimental findings from [1] as shown in Fig. 8(b). It can be seen that the back stress is significantly higher than the effective stress, which is also aligned with experimental findings reported in [61]. The simulated trends are in good agreement with the experimental data, although discrepancies with exact values are noticed, especially for the effective stress, which might stem from the texture changing during the manufacturing process.

3.3.2. *Effect of NG volume content*

The developed model was further applied to study the uniaxial tensile properties of copper-based HSLs with different NG volume content and the simulated results compared against the experimental investigation presented in [7]. The modelling details follow the experimental set up described in [7] for post mortem comparisons; specifically the volume content of the NG layer is set to 0.1, 0.22 and 0.47 while the thickness of the specimen was 600 μm.

Fig. 9 shows the comparisons of the stress–strain curves with different NG volume contents between the theoretical predictions obtained in this work by implementing 1) the modified ROM method, 2) the classical ROM predictions [6] and 3) the experimental results [7]. The predicted results using the modified ROM method are slightly larger than those from the classical ROM predictions in all cases. This is because the effect of IAZs is not included in the ROM method. Generally, the simulated stress–strain curves for all considered NG volume contents agree well with the experimental results [7] and the ROM predictions

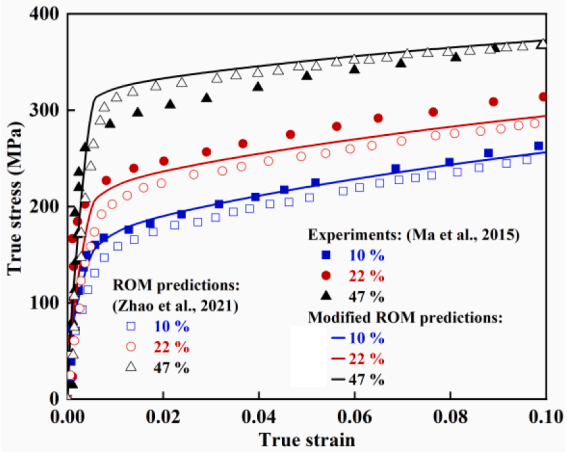

Fig. 9. Comparison of the results obtained between the modified ROM method predictions, ROM results from [6] and experimental results from [7] for laminates with different volume content of NG layer.

[6]. The reason why the ROM method is also well-aligned with the experimental results here is likely due to the fact that the IAZs take up only 1.9 %, 2.1 % and 3.1 % of the CG layer, for the respective volume contents investigated, and thus, can be considered to have a negligible effect on the overall properties.

3.3.3. *Outcomes from the integrated FEM model developed in this research*

The previous two sections investigated the effectiveness of the classical ROM approach and the modified ROM method from Zhao and co-workers [6] to quantitatively predict the effect of the layer thickness and of the NG volume content on the tensile response of copper-based HSLs. However, experimental data [7] show that the synergetic effect of the NG and CG layers would produce a more significant strengthening than that inferred by the weight-based mathematical formulae that characterise both methods. Besides, the CG and NG layers experience different damage characteristics when considered as standalone entities compared to when they compose a HSL stack. To shed further light on the constraints and the synergy of the NG and CG layers, an integrated FEM model is developed to study the mechanical response of the 'sandwich structure' of HSL materials rather than studying the separate standalone layers.

One should notice that for homogenous grained copper, a Taylor constant M of 3.06 is adopted for the CG, the NG and the IAZ material. However, the laminates are manufactured by HPT, rolling and annealing which would result in a different grain size for final specimens, especially for the NG layers [1,6]. In consideration of this, a Taylor constant of 2.45 is adopted for the NG layer in the laminates following the study presented in [62] while the rest of the material properties remain unchanged. The model consists of three regions, namely the CG, the NG and the IAZs, as previously illustrated in Fig. 1(b). These regions were geometrically modelled to adhere to the experimental conditions of [1,7] and were meshed suitably. The predicted stress–strain curves using the integrated FEM model of copper-based HSLs with different layer thicknesses and NG volume contents are plotted in Fig. 10. This figure also includes experimental data from [1,7] for comparison purpose. The simulated stress–strain curves with different layer thicknesses correlate relatively well with experimental values. Similar to what was found earlier when implementing the modified ROM method from Zhao and co-workers [6], the larger the layer thickness, the better the approximation. This indicates again the crucial role of interfaces and the IAZ. For the laminates with different NG volume contents, i.e., Fig. 10(b), the simulated stress–strain curves also agree relatively well with experimental data for all considered scenarios. As discussed earlier, the IAZs content considered for all simulations in this figure is lower than that for the simulations Fig. 10(a) where the layer thickness is small and thus, a better correlation can be achieved. This figure also indicates that the mutual constraints between the NG and CG layer are negligible in the scenarios modelled in Fig. 10(b) because the results displayed are close to the results in Fig. 9.

To investigate the mutual interactions between the NG and the CG layers, the lateral stress distribution, of the laminates with 10 %, 22 % and 47 % NG volume content at the true strain of 0.5 % is shown in Fig. 11 together with the numerical results from Zhao et al. [6] for comparison. Experimental observations at this stage report that the CG layer has yielded while the deformation in the NG layer is still pre-yield, i.e., elastic [46]. The selected simulation path in the presented work corresponds to the middle section of the specimen along the thickness direction as shown in the inset of Fig. 11(b). The presented results agree well with the numerical findings of [6] where 5 different paths on the cross section were selected. The lateral stress is negative in the NG region while positive in the CG region. This reveals the severe 'shrinkage' of the NG layer along the lateral direction and the multiaxial loading in the HSL structure. This incompatibility between the NG and the CG layers during deformation was also reported in the experiments conducted in [1]. The lateral stress distribution in the CG layer was found to be around 5 MPa which is close to the results reported in [21,38], while the lateral stress distribution in the NG layer can be relatively high, such as −25 MPa. It can also be observed from Fig. 11(b) that the smaller the NG volume content, the larger the difference in lateral stress between the CG and NG layers. This indicates that a smaller NG volume content would lead to a larger incompatibility between both layers. This bi-axial stress state can activate more slip systems and contributes to extra strengthening beyond the predictions made using the ROM method [63].

In the integrated FEM model developed here, the NG layer in the HSL displays no necking in the first 10 % true strain (see Fig. 12(b)) while the stand-alone NG layer started necking at 0.4 % true strain (see earlier Fig. 5(a)). A similar phenomenon was observed in the experiments conducted in [7] where the NG layer in the laminates started necking at the strain of 12 % while the stand-alone NG layer counterpart yielded at an early strain of 0.7 %. The maximum JC damage accumulation factor in the NG layer of the copper based HSL composite was simulated to be around 0.0065 for all layer thicknesses considered at a strain of 10 %, as shown in Fig. 12(a). This is significantly smaller than that in standalone NG layer, which was found to be 0.06 (c.f. Fig. 6(a)) for the same value of strain. This is explained by the fact that early necking of the NG layer in HSL structures is suppressed by the CG layers through the formation of two IAZs on both sides [46]. The early tensile failure exhibited in a standalone NG specimen is thus avoided. The damage accumulation factor in the NG layer for different thicknesses is also displayed with Fig. 12(a). It can be seen that the smaller the layer thickness, then the smaller the damage factor. This indicates that the NG layer is protected

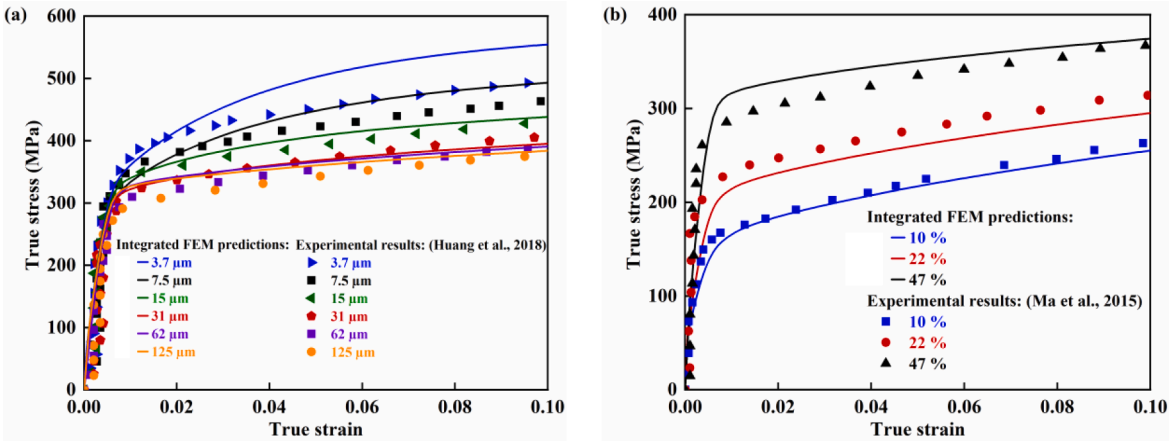

Fig. 10. (a) Plots of simulated stress–strain curves for copper-based HSLs using the integrated FE model with (a) different layer thicknesses against experimental results from [1] and (b) different NG volume contents against experimental results from [7].

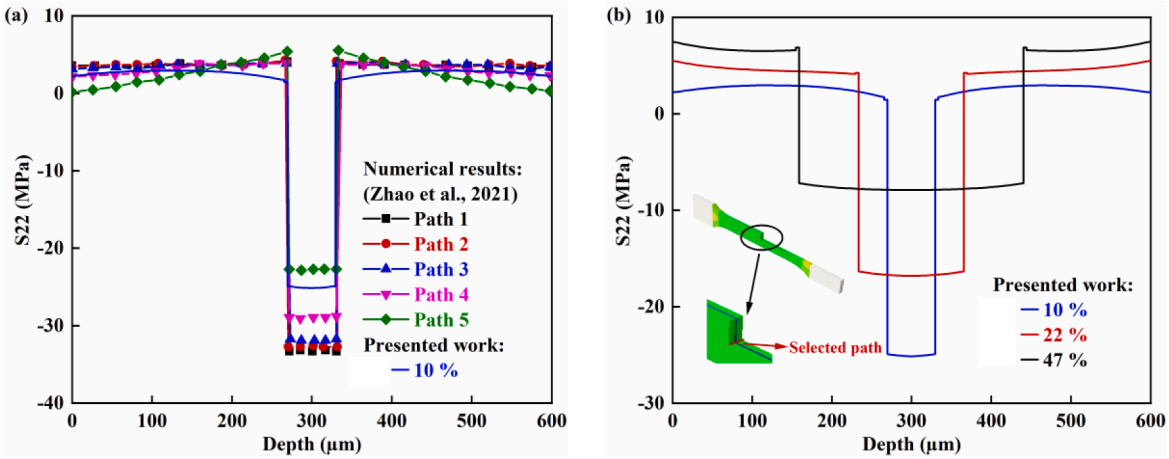

Fig. 11. (a) Comparisons of simulated lateral stress distribution of 10 % NG volume content of a copper-based HSL at the true strain of 0.5 % with numerical results presented in [6]; (b) lateral stress distribution of simulated copper-based HSLs with different NG volume contents at the true strain of 0.5 %.

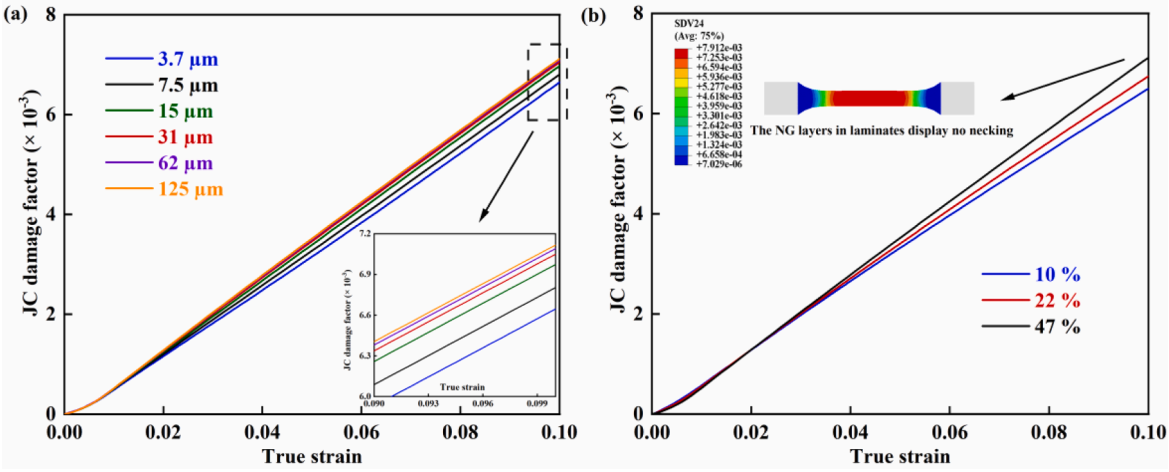

Fig. 12. (a) The simulated JC damage accumulation factor of the NG layer in HSLs with layers of different thicknesses, (b) The simulated JC damage accumulation factor of the NG layer in HSLs with 10 %, 22 % and 47 % NG volume content using the integrated FE model developed in this research.

by the neighbouring layers since the smaller layer thickness means a larger interface/IAZs density. The damage factor in the NG layer for copper-based HSLs with different volume contents is given with Fig. 12 (b). As reported above, the damage factor in this situation is about one magnitude smaller than that for a standalone NG layer, which indicates that the neighbouring IAZs and CG layer alleviates the stress concentration. However, with the increase in the volume content of the NG layer, the stress concentration cannot ultimately be lessened. This leads to a larger damage factor and thus, an earlier failure as observed in experiments conducted in [7].

The numerical results presented in this work using the modified ROM method from Zhao and co-workers [6] and the developed integrated FEM model, including the output stress–strain curves, microhardness, back stress and JC damage factors correlate well with the corresponding experimental observations. However, the simulated stress–strain curves in Fig. 7(a) and 10(a) for the copper-based HSL with different layer thicknesses still somewhat show some degree of discrepancy with experimental values. A first possible reason behind this outcome may be due to the uncertainty around the thickness of IAZs as various values are reported in the literature, i.e. 5 μm to 6 μm in [1] and the size of one coarse grain in [6]. A second possible source of error may be linked to the uncertainty in the value of the Poisson's ratio of the CG layer in the integrated HSL structure simulations. More specifically, findings from [63] suggest that the Poisson's ratio of this layer changed from 0.36 to 0.5 to accommodate the mechanical incompatibility between layers. As a result, the uniaxial tensile loading turns into a bi-axial one and more slip systems are activated which contribute to the extra strengthening [21]. The interaction between the NG and CG layers is found to make a significant contribution to back stress [16] and this synergetic hardening behaviour needs to be further investigated. In addition, the cohesive interfaces between different layers were not included but modelled as a whole part in this research, which will ineluctably lead to deviations of the laminate properties.

While this work focusses on the heterogenous deformation-induced hardening, the hardening of such structures [24] might also stem from various sources such as the additive effect of individual layer by forest hardening as in gradient structures, compressive residual stress induced strain hardening, and partly recovered forest dislocation hardening due to the change of stress state in the NG layer. The change in grain size in different layers during the deformation process and due to the manufacturing process as well as nanotwin boundary-mediated strain hardening might contribute to deviations as well. For example, grain coarsening in the NG layer of gradient copper was observed in [64] and 'strain softening' was induced as a result. Consequently, an enhanced strength-ductility synergy was achieved. In future studies, the evolution of grain size should be modelled as a function of temperature and stress–strain rate to achieve more accurate predictions. In addition to this, damage initiation and fracture are a complicated process especially

in such 'sandwich' structures where necking-delayed ductile mode to necking-inhibited brittle mode transition [56], interface delamination and slip bands activities [5] are involved. The inclusion of cohesive interfaces with reasonable progressive failure criterion has the potential to lead to further advances when investigating this problem.

4. Conclusions

A novel multiple physical mechanisms based constitutive model coupled with the Johnson Cook damage criterion was developed to simulate the deformation of heterogeneous-structured laminates (HSLs). The proposed approach enables quantitative information about the internal damage in HSLs to be obtained and investigated in real-time. The evolution of geometrically necessary dislocations, statistically stored dislocations and resulting back stress were taken into account using dislocation pile up theory. The simulated microhardness, stress–strain curves and back stress evolution agreed well with published experimental results. The important conclusions that can be drawn from this work are as follows:

(1) The developed HSL simulation model is considered to outperform the traditional rule of mixture (ROM) and the modified ROM methods due to its ability to investigate the interactive constraints between the coarse-grained (CG) and nano-grained (NG) layers and to quantify damage conditions throughout the deformation process.
(2) Given the ability of the developed model to evaluate the damage accumulation factor in the NG layer, simulations outcomes were obtained which aligned with the following known experimental observations: 1) the smaller the layer thickness, then the smaller the internal damage and 2) the internal damage increases with the increase in volume content of the NG layer.
(3) For a set simulated strain of 10 %, it was found that the damage accumulation factor in the NG layer was 10 times lower than that in a stand-alone NG layer not sandwiched between two CG layers. This confirms that protection of the NG layers is provided by the CG layers during deformation in HSLs.
(4) Deviations from experimental data were observed when predicting the stress–strain curves of HSLs with smaller layer thickness values using both the developed model and the modified ROM method. It is probable that the inclusion of interfaces and a reasonable traction-separation progressive failure law in the proposed FEM model should have the potential to address this issue.

It is anticipated that the developed framework could be easily adopted to simulate other metallic heterogeneous materials especially in the context of dynamic manufacturing processes, such as forming. In addition, the proposed method could support recent as well as future developments of new heterogeneous structured materials as progress made in additive manufacturing of metallic materials provide promising perspectives for the production of such metallic composites. Future applications of this class of materials could span from aerospace, biomedical engineering through to energy [65–67]. Thus, the proposed framework should support the application of metallic laminates, and potentially gradient metallic structures too, by facilitating the optimal design of such materials.

CRediT authorship contribution statement

Shuai Zhu: Conceptualization, Formal analysis, Investigation, Methodology, Software, Writing – original draft, Writing – review & editing. **Emmanuel Brousseau:** Formal analysis, Methodology, Resources, Supervision, Writing – review & editing. **Yiyu Shao:** Formal analysis, Investigation, Software. **Wenfei Peng:** Formal analysis, Investigation, Software.

Declaration of competing interest

The authors declare that they have no known competing financial interests or personal relationships that could have appeared to influence the work reported in this paper.

Data availability

Data will be made available on request.

Acknowledgement

Shuai Zhu would like to thank the support of China Scholarship Council for sponsoring his PhD study at Cardiff University. This research was undertaken using the supercomputing facilities at Cardiff University operated by Advanced Research Computing at Cardiff (ARCCA) on behalf of the Cardiff Supercomputing Facility and the HPC Wales and Supercomputing Wales (SCW) projects. We acknowledge the support of the latter, which was part-funded by the European Regional Development Fund (ERDF) via the Welsh Government. This work was supported by the Fundamental Research Funds for the Provincial Universities of Zhejiang (No. SJLZ 2021002) and the Ningbo Science and Technology Innovation 2025 Major Project (2021Z099, 2019B10100). Shuai Zhu would like to thank Dr Jianfeng Zhao, Dr Xu Zhang, Dr Emilio Martínez Pañeda, Dr Yin Zhang, Dr Oliver Pantale, Dr David Morin and Dr Martin Baeker for their inspiration. The authors are open to possible collaborations and the developed subroutines (classic_JC_dynamic_damage.f, JC_dynamic_damage_MSGP.f), (multi_mechanism_MSGP.f) and ABAQUS inp files in this work are available upon reasonable requests (email: zhushuaihit0712@gcom).

References

[1] Huang CX, Wang YF, Ma XL, Yin S, Höppel HW, Göken M, et al. Interface affected zone for optimal strength and ductility in heterogeneous laminate. Mater Today 2018;21:713–9.
[2] Li J, Wang S, Mao Q, Huang Z, Li Y. Soft/hard copper/bronze laminates with superior mechanical properties. Mater Sci Eng A 2019;756:213–8.
[3] Ma X, Huang C, Moering J, Ruppert M, Höppel HW, Göken M, et al. Mechanical properties of copper/bronze laminates: role of interfaces. Acta Mater 2016;116:43–52.
[4] Liang F, Luo X-M, Zhang G-P. Interface-coupling-dependent mechanical behaviors of sandwich-structured Ni/Cu/Ni composites. Mater Sci Eng A 2019;743:436–44.
[5] Zhao Y, Wang T, Gao B, Gao Z, Han J, Zhang S, et al. Towards enhanced strength-ductility in pure copper by fabricating hetero grain composite laminates. J Alloy Compd 2022;928:167192.
[6] Zhao J, Zaiser M, Lu X, Zhang B, Huang C, Kang G, et al. Size-dependent plasticity of hetero-structured laminates: a constitutive model considering deformation heterogeneities. Int J Plast 2021;145:103063.
[7] Ma XL, Huang CX, Xu WZ, Zhou H, Wu XL, Zhu YT. Strain hardening and ductility in a coarse-grain/nanostructure laminate material. Scr Mater 2015;103:57–60.
[8] Kümmel F, Kreuz M, Hausöl T, Höppel HW, Göken M. Microstructure and mechanical properties of accumulative roll-bonded AA1050A/AA5005 laminated metal composites. Metals 2016.
[9] Zhao J, Lu X, Liu J, Bao C, Kang G, Zaiser M, et al. The tension-compression behavior of gradient structured materials: a deformation-mechanism-based strain gradient plasticity model. Mech Mater 2021;159:103912.
[10] Semiatin SL, Piehler HR. Deformation of sandwich sheet materials in uniaxial tension. Metall Trans A 1979;10:85–96.
[11] Nyung Lee D, Keun KY. Tensile properties of stainless steel-clad aluminium sandwich sheet metals. J Mater Sci 1988;23:1436–42.
[12] Koumoulos EP, Jagadale P, Lorenzi A, Tagliaferro A, Charitidis CA. Evaluation of surface properties of epoxy–nanodiamonds composites. Compos B Eng 2015;80:27–36.
[13] Zha C, Hu J, Li A, Huang S, Liu H, Chen G, et al. Nanoindentation study on mechanical properties and curing depth of dental resin nanocomposites. Polym Compos 2019;40:1473–80.
[14] Karimzadeh A, Ayatollahi MR. Investigation of mechanical and tribological properties of bone cement by nano-indentation and nano-scratch experiments. Polym Test 2012;31:828–33.
[15] Karimzadeh AR, Koloor SS, Ayatollahi MR, Bushroa AR, Yahya MY. Assessment of nano-indentation method in mechanical characterization of heterogeneous nanocomposite materials using experimental and computational approaches. Sci Rep 2019;9:15763.

[16] Wang Y, Yang M, Ma X, Wang M, Yin K, Huang A, et al. Improved back stress and synergetic strain hardening in coarse-grain/nanostructure laminates. Mater Sci Eng A 2018;727:113–8.
[17] Zhao W, Liao H, Lun Y, Zhang S, Song B. Role of interfaces in the deformation behavior of lamellar TiAl-based alloys with CPFEM simulation. Mater Today Commun 2022;32:103942.
[18] Zhao J, Kan Q, Zhou L, Kang G, Fan H, Zhang X. Deformation mechanisms based constitutive modelling and strength-ductility mapping of gradient nano-grained materials. Mater Sci Eng A 2019;742:400–8.
[19] Fang Q, Li L, Li J, Wu H. Strengthening mechanism of gradient nanostructured body-centred cubic iron film: from inverse hall-petch to classic hall-petch. Comput Mater Sci 2018;152:236–42.
[20] Yuan R, Du H. Modeling the effects of interface spacing on the mechanical properties of heterogeneous laminates. Comput Mater Sci 2020;173:109391.
[21] Wu XL, Jiang P, Chen L, Zhang JF, Yuan FP, Zhu YT. Synergetic strengthening by gradient structure. Materials Research Letters 2014;2:185–91.
[22] Li J, Soh AK. Modeling of the plastic deformation of nanostructured materials with grain size gradient. Int J Plast 2012;39:88–102.
[23] Li J, Weng GJ, Chen S, Wu X. On strain hardening mechanism in gradient nanostructures. Int J Plast 2017;88:89–107.
[24] Wu X, Zhu Y, Lu K. Ductility and strain hardening in gradient and lamellar structured materials. Scr Mater 2020;186:321–5.
[25] Johnson GR, Cook WH. Fracture characteristics of three metals subjected to various strains, strain rates, temperatures and pressures. Eng Fract Mech 1985;21:31–48.
[26] Lai X, Li H, Li C, Lin Z, Ni J. Modelling and analysis of micro scale milling considering size effect, micro cutter edge radius and minimum chip thickness. Int J Mach Tool Manu 2008;48:1–14.
[27] Wang Z, Zhang H, Li Z, Li G, Zhang J, Zhang J, et al. Crystal plasticity finite element simulation and experiment investigation of nanoscratching of single crystalline copper. Wear 2019;430–431:100–7.
[28] Guo X, Ji R, Weng GJ, Zhu LL, Lu J. Micromechanical simulation of fracture behavior of bimodal nanostructured metals. Mater Sci Eng A 2014;618:479–89.
[29] Guo X, Sun X, Tian X, Weng GJ, Ouyang QD, Zhu LL. Simulation of ballistic performance of a two-layered structure of nanostructured metal and ceramic. Compos Struct 2016;157:163–73.
[30] Huang Y, Qu S, Hwang KC, Li M, Gao H. A conventional theory of mechanism-based strain gradient plasticity. Int J Plast 2004;20:753–82.
[31] Hirth JP, Lothe J, Mura T. Theory of Dislocations (2nd ed.). Journal of Applied Mechanics. 1983 50 476.
[32] Yayli MÖ. A compact analytical method for vibration of micro-sized beams with different boundary conditions. Mech Adv Mater Struct 2016;24:496–508.
[33] Yayli MÖ. Free longitudinal vibration of a nanorod with elastic spring boundary conditions made of functionally graded material. Micro & Nano Letters 2018;13:1031–5.
[34] Yayli MÖ. Free vibration analysis of a rotationally restrained (FG) nanotube. Microsyst Technol 2019;25:3723–34.
[35] Lele SP, Anand L. A small-deformation strain-gradient theory for isotropic viscoplastic materials. Phil Mag 2008;88:3655–89.
[36] Lele SP, Anand L. A large-deformation strain-gradient theory for isotropic viscoplastic materials. Int J Plast 2009;25:420–53.
[37] Taylor GI. The mechanism of plastic deformation of crystals. Part I.—theoretical. Proceedings of the Royal Society of London Series A, Containing Papers of a Mathematical and Physical Character 1997;145:362–87.
[38] Zhao J, Lu X, Yuan F, Kan Q, Qu S, Kang G, et al. Multiple mechanism based constitutive modeling of gradient nanograined material. Int J Plast 2020;125:314–30.
[39] Sinclair CW, Poole WJ, Bréchet Y. A model for the grain size dependent work hardening of copper. Scr Mater 2006;55:739–42.
[40] Nye JF. Some geometrical relations in dislocated crystals. Acta Metall 1953;1:153–62.
[41] Ashby MF. The deformation of plastically non-homogeneous materials. The Philosophical Magazine: A Journal of Theoretical Experimental and Applied Physics 1970;21:399–424.
[42] Fleck NA, Hutchinson JW. Strain gradient plasticity. Adv Appl Mech 1997;33:295–361.
[43] Kocks UF. Laws for work-hardening and low-temperature creep. J Eng Mater Technol 1976;98:76–85.
[44] Mecking H, Kocks UF. Kinetics of flow and strain-hardening. Acta Metall 1981;29:1865–75.
[45] Estrin Y. Dislocation theory based constitutive modelling: foundations and applications. J Mater Process Technol 1998;80–81:33–9.
[46] Wu X, Zhu Y. Heterogeneous materials: a new class of materials with unprecedented mechanical properties. Materials Research Letters 2017;5:527–32.
[47] Murr LE. Dislocation ledge sources: dispelling the myth of frank-read source importance. Metall Mater Trans A 2016;47:5811–26.
[48] Antunes JM, Fernandes JV, Menezes LF, Chaparro BM. A new approach for reverse analyses in depth-sensing indentation using numerical simulation. Acta Mater 2007;55:69–81.
[49] Antunes JM, Menezes LF, Fernandes JV. Three-dimensional numerical simulation of vickers indentation tests. Int J Solids Struct 2006;43:784–806.
[50] Sakharova NA, Fernandes JV, Antunes JM, Oliveira MC. Comparison between berkovich, vickers and conical indentation tests: a three-dimensional numerical simulation study. Int J Solids Struct 2009;46:1095–104.
[51] Olfe J, Neuhäuser H. Dislocation groups, multipoles, and friction stresses in α-CuZn alloys. Physica Status Solidi (a) 1988;109:149–60.
[52] Champion Y, Langlois C, Guérin-Mailly S, Langlois P, Bonnentien J-L, Hÿtch MJ. Near-perfect elastoplasticity in pure nanocrystalline copper. Science 2003;300:310–1.
[53] Dasharath SM, Mula S. Mechanical properties and fracture mechanisms of ultrafine grained Cu-9.6% Zn alloy processed by multiaxial cryoforging. Mater Sci Eng A 2016;675:403–14.
[54] Zhao Y, Zhu Y, Liao X, Horita Z, Langdon TG. Tailoring stacking fault energy for high ductility and high strength in ultrafine grained Cu and its alloy. Appl Phys Lett 2006;89:121906.
[55] Wang YF, Wang MS, Fang XT, Guo FJ, Liu HQ, Scattergood RO, et al. Extra strengthening in a coarse/ultrafine grained laminate: role of gradient interfaces. Int J Plast 2019;123:196–207.
[56] Liang F, Tan H-F, Zhang B, Zhang G-P. Maximizing necking-delayed fracture of sandwich-structured Ni/Cu/Ni composites. Scr Mater 2017;134:28–32.
[57] Fan M, Domblesky J, Jin K, Qin L, Cui S, Guo X, et al. Effect of original layer thicknesses on the interface bonding and mechanical properties of TiAl laminate composites. Mater Des 2016;99:535–42.
[58] Fan G, Geng L, Wu H, Miao K, Cui X, Kang H, et al. Improving the tensile ductility of metal matrix composites by laminated structure: a coupled X-ray tomography and digital image correlation study. Scr Mater 2017;135:63–7.
[59] Yang M, Pan Y, Yuan F, Zhu Y, Wu X. Back stress strengthening and strain hardening in gradient structure. Materials Research Letters 2016;4:145–51.
[60] Gao H, Huang Y, Nix WD, Hutchinson JW. Mechanism-based strain gradient plasticity— I. theory. J Mech Phys Solids 1999;47:1239–63.
[61] Ren J, Zhang Y, Zhao D, Chen Y, Guan S, Liu Y, et al. Strong yet ductile nanolamellar high-entropy alloys by additive manufacturing. Nature 2022;608:62–8.
[62] Starink MJ, Wang SC. A model for the yield strength of overaged Al–Zn–Mg–Cu alloys. Acta Mater 2003;51:5131–50.
[63] Wu X, Jiang P, Chen L, Yuan F, Zhu YT. Extraordinary strain hardening by gradient structure. Proc Natl Acad Sci 2014;111:7197–201.
[64] Chen W, You ZS, Tao NR, Jin ZH, Lu L. Mechanically-induced grain coarsening in gradient nano-grained copper. Acta Mater 2017;125:255–64.
[65] Nazir A, Gokcekaya O, Md Masum Billah K, Ertugrul O, Jiang J, Sun J, et al. Multi-material additive manufacturing: a systematic review of design, properties, applications, challenges, and 3D printing of materials and cellular metamaterials. Mater Des 2023;226.
[66] Shuai C, Li D, Yao X, Li X, Gao C. Additive manufacturing of promising heterostructure for biomedical applications. International Journal of Extreme Manufacturing 2023;5:032012.
[67] Wei C, Zhang Z, Cheng D, Sun Z, Zhu M, Li L. An overview of laser-based multiple metallic material additive manufacturing: from macro- to micro-scales. International Journal of Extreme Manufacturing 2021;3:012003.
[68] Zhu L, Ruan H, Chen A, Guo X, Lu J. Microstructures-based constitutive analysis for mechanical properties of gradient-nanostructured 304 stainless steels. Acta Materialia 2017;128:375–90.